



Transport properties of kaolin limestone blend and hybrid slag blend high-strength self-compacting concrete

Selesca Devi Selvaraj¹ , Shanmugapuram Subramanian Vivek¹ 

¹SASTRA Deemed University, School of Civil Engineering, 613 401, Thanjavur, Tamil Nadu, India.

e-mail: selescadevi@civil.sastra.ac.in, vivek@civil.sastra.edu

ABSTRACT

This study aims to develop a high-strength, high-performance self-compacting concrete through sustainable cement replacement using tailor-made supplementary cementitious materials. Two blends were formed: a hybrid slag blend consisting of ultrafine slag and ground granulated blast furnace slag in a 2:1 ratio with 1.5% gypsum, and a kaolinite-limestone blend combining calcined kaolin and limestone powder with different origins in a 2:1 ratio with 1% gypsum. Material selection was based on the chemical compatibility with the cement to ensure synergistic behavior. Durability characteristics were evaluated through water absorption, porosity, sorptivity, and rapid chloride penetration tests, while microstructural characteristics were analysed using SEM, XRD, and FTIR analyses. The HSB mix, at 30% replacement, significantly improved durability by reducing water absorption and porosity, and enhancing chloride resistance. The KLB mixes exhibited superior performance up to 50% replacement, with the volume of permeable voids decreasing from 2.71% to 1.35% at 28 days and from 2.62% to 1.05% at 90 days, respectively. The sorptivity index followed a similar declining trend, and chloride penetration in KLB at 50% mix remained negligible across all curing periods. XRD analysis confirmed a reduction of clinker phases, while FTIR revealed the formation of stable carboaluminate phases in KLB mixes, enhanced durability.

Keywords: Sorptivity; porosity; water absorption; rapid chloride penetration test; gypsum.

1. INTRODUCTION

High-strength self-compacting concrete (HS-SCC) has gained considerable attention in modern construction due to its self-compacting abilities, which make it ideal for complex structural elements and densely reinforced sections with focusing on both mechanical properties and superior flowability. However, while strength and workability have traditionally been the primary focus in the development of HS-SCC, durability properties are equally critical to ensure long-term performance and sustainability. Durability refers to the concrete's resistance to environmental, chemical, and mechanical degradation over time. Therefore, the concrete must have not only the mechanical requirements but also the durability expectations. Several studies focusing on the durability performance of SCC have been reported, including recent publications in this journal, which emphasize the importance of this research direction [1–2]. The issue of durability is often overlooked, as engineers commonly assume that high-strength concrete inherently possesses adequate durability. Concrete structures are susceptible to deterioration caused by both physical and chemical mechanisms. The understanding of pore structure within the hardened cement paste is essential for evaluating the transport properties of cementitious materials. The pore structure within cement-based materials is not static, as the unhydrated cement particles react with water during cement hydration and develop a new and denser pore network [3]. After the solid matrix forms, a critical factor influencing material properties is the connectivity of the remaining pores, as it explains how transport properties are governed by the pathways linking voids and pores in the cement paste matrix and the interfacial transition zone (ITZ) [4–5].

Self-compacting concrete (SCC) requires a higher content of fine materials than conventional concrete, which typically results in increased cement usage [6]. However, the inclusions of supplementary cementitious materials (SCMs) significantly enhance the durability and mechanical performance of SCC while simultaneously reducing cement consumption [7]. Beyond improving strength and mitigating the effects of insufficient compaction, SCMs offer economic and sustainability benefits [8]. Materials such as silica fume, fly ash, GGBS, metakaolin, and rice husk ash are commonly employed for this purpose [9]. For cost efficiency, some studies

have also focused on incorporating agricultural waste ashes, not only as a partial cement replacement but also as an alternative to conventional aggregate [10]. Durability enhancement in SCC primarily results from pozzolanic reactions during cement hydration, wherein SCMs react with calcium hydroxide (CH), a weak, soluble by-product, to generate additional calcium silicate hydrate (CSH) gel. As CH readily dissolves upon water ingress, it increases porosity and accelerates chemical degradation [11]. The consumption of CH by SCMs thus refines the pore structure, reduces pore connectivity, and lowers permeability, significantly improving the long-term durability and resistance of SCC to aggressive environments. While most SCC studies involving SCMs emphasize strength improvement, several have explored their influence on fresh and durability properties. CHANDRU *et al.* [12] reported that a ternary blend of 10% silica fume and 20% GGBS improved the workability of SCC due to the inclusion of induced furnace slag (IFS) aggregate. However, replacing natural aggregates with IFS reduced the compressive strength from 53 MPa to 44 MPa. In a follow-up study, CHANDRU *et al.* [13] noted that although IFS enhanced flow characteristics, it led to 16–25% higher permeable voids, reducing durability. Still, a ternary blend with 5% silica fume and 60% GGBS achieved a 44% reduction in water absorption and a 27% reduction in permeable voids. SCC used in binary and ternary mixes using 40% fly ash and 10% silica fume outperformed conventional SCC in terms of mechanical strength [14]. BIRGONDA and KATHIKEYAN [15] evaluated a quaternary blend containing fly ash, silica fume, and GGBS. Although early-age strength was lower than in conventional SCC, strength improved at later ages, achieving 50 MPa at 56 days. Moreover, the cost of SCC was reduced by 19–25% using the quaternary blend. Regarding durability, SCC incorporating up to 40% GGBS, 2.5% silica fume, and 10% fly ash showed marked improvements, including 25% lower water absorption, 24% pore volume reduction, and 46% sorptivity reduction, which also enhanced electrical resistivity and energy efficiency [16]. However, mixes with SCM replacement levels exceeding 50% often showed increased carbonation depth, indicating reduced carbonation resistance [17]. Despite these promising results, they often continue to rely heavily on conventional materials, achieving only limited reductions in clinker content. Addressing this gap is essential for advancing the sustainability of high-performance SCC. To this end, the present study proposes two tailor-made SCM blends to support higher levels of cement replacement without compromising concrete performance. The first blend, termed as Hybrid Slag Blend (HSB), which utilizes materials of similar origin but differing fineness, that is, two parts ultrafine slag and one part GGBS, combined with 1.5% gypsum at each replacement level. This combination is intended to improve the particle packing density. The second blend, known as Kaolin-Limestone Blend (KLB), combines materials of different origins to emulate the mineralogical composition of cement. It consists of two parts calcined kaolin and one part limestone powder, with 1% gypsum at every replacement level. Both blends are formulated using abundantly available materials to offer a practical and sustainable approach to cement reduction. Since most SCMs are industrial by-products, their hydration activity is largely secondary, driven by pozzolanic or latent hydraulic reactions. As a result, significant strength gains are often observed at later curing ages, particularly around 90 days [18]. As HS-SCC is commonly used in critical structures such as bridges and marine piers, assessing its resistance to chloride ingress and capillary absorption becomes essential. In this study, the addition of KLB resulted in compressive strength improvements from 59 MPa to 69 MPa at 28 days and from 65 MPa to 76 MPa at 90 days, when the replacement level increased from 10% to 40%. Similarly, HSB blends showed strength gains from 59 MPa to 67 MPa at 28 days and from 65 MPa to 73 MPa at 90 days, at replacement levels ranging from 10% to 30%. These results confirm that the mixes fall within the HS-SCC.

2. MATERIALS AND METHODOLOGY

2.1. Materials used in this study

Ordinary Portland cement (OPC) of 53 grade, conforming to IS 12269 [19], was used as the primary binder. Manufactured sand (M-sand) classified under Zone II grading was taken as the fine aggregate (FA), while crushed gravel with a maximum size of 12.5 mm was used as the coarse aggregate (CA). Both aggregates were tested under IS 383 [20]. The mineral admixtures used in this study include calcined kaolin (CK), limestone powder (LP), ground granulated blast furnace slag (GGBS), ultrafine slag (UFS), and gypsum (GY), all of which were sourced from ASTTRA Chemicals, Chennai, as shown in Figure 1. The physical properties of these materials, as provided by the supplier, are listed in Table 1. The chemical compositions of the materials are listed in Table 2. For enhanced workability and mix stability, a polycarboxylate-based superplasticizer conforming to ASTM C494 [21] was used, along with a viscosity-modifying agent (VMA), specifically Auramix V200.

2.2. Methodology

The M60-grade concrete mix was proportioned according to IS 10262 [22]. Two series of mixes were developed by partial replacement of cement with tailor-made SCMs, that is, the hybrid slag blend and the kaolin-limestone



Figure 1: Materials used in this study.

Table 1: Physical properties of mineral admixtures.

PHYSICAL PROPERTIES	GGBS	UFS	CK	LP	GY
Specific gravity	2.85	2.7	2.63	2.65	2.4
Bulk density (kg/m ³)	1200	700	800	1200	950
Appearance	Light grey	Grey	White powder	White grey	Pure white

Table 2: Elemental compositions of the cementitious materials (%).

ELEMENTS IN OXIDE FORM	CEMENT	GGBS	UFS	CK	LP	GY
SiO ₂	23.2	36.45	34.12	43.87	10.21	1.98
Fe ₂ O ₃	3.4	0.97	0.19	0.58	1.20	0.24
Al ₂ O ₃	4.15	13.6	26	36.59	3.72	0.6
CaO	64	32.05	40	0.25	80	30.36
MgO	1.53	5.37	7.73	0.12	2.16	0.82
Na ₂ O	0.42	0.03	0.36	0.31	0.18	0.02
K ₂ O	1.34	0.55	1.13	0.07	0.41	0.04
SO ₃	2.16	—	—	—	—	41.62
Loss on ignition	1.7	1.02	0.58	—	—	20.15

blend. In the HSB series, cement was replaced at levels of 10% to 50%, denoted as HSB0.10 to HSB0.50, where HSB0.10 represents a 10% replacement. Similarly, the KLB involved cement replacement from 10% to 50% and was denoted as KLB0.10 to KLB0.50. Each mix was optimized by adjusting the dosage of superplasticizer and viscosity-modifying agent until the fresh properties met the EFNARC guidelines [23]. The HSB binder was prepared by combining GGBS and ultrafine slag in a 2:1 ratio with 1.5% gypsum powder. In both blends, the selection of finer materials in higher proportions was intentional, as SCC demands more fines to ensure proper flowability and particle packing, making CK and UFS suitable primary components in these tailor-made SCM systems from Figure 2. The complete mix proportions for both HSB and KLB mixes, along with the conventional high-strength self-compacting concrete (CONV), are provided in Tables 3 and 4. Both HSB and KLB binders exhibit high alumina oxide content, which accelerates hydration and contributes to early loss of plasticity in the paste [24–25]. To counterbalance this effect, gypsum was added to regulate the setting behavior. However, excessive gypsum can lead to the formation of excessive ettringite, increasing the risk of internal cracking [26].

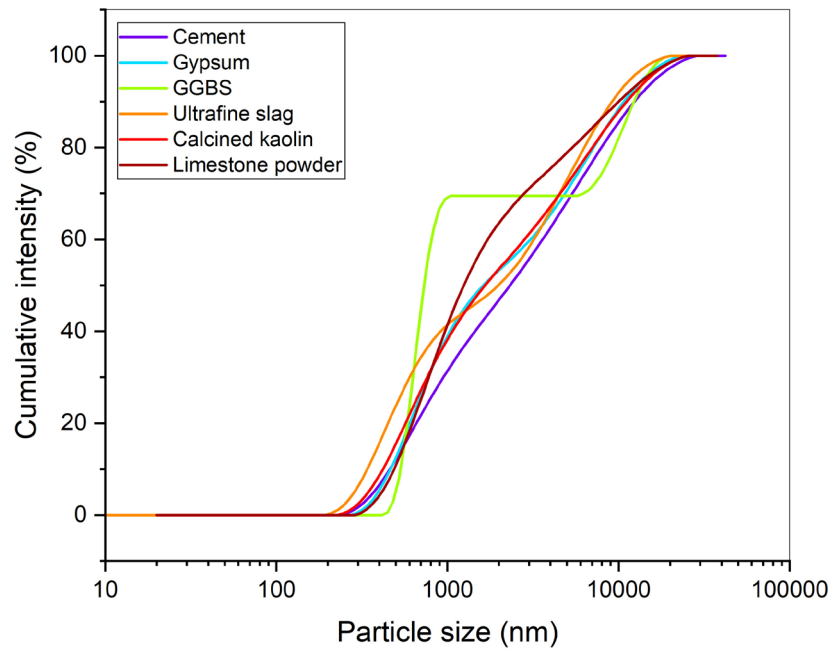


Figure 2: Particle size distribution for the cementitious materials.

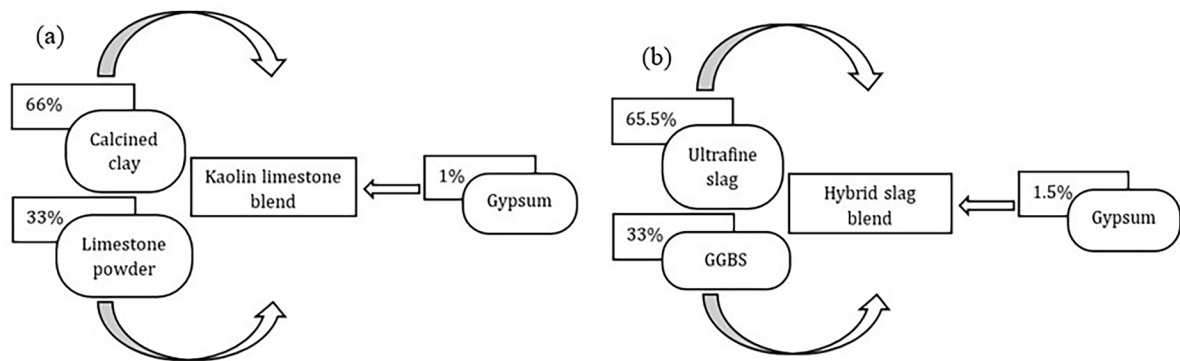


Figure 3: Preparation of tailor-made SCMs.

Table 3: Mix proportions for HSB and KLB mixes (kg/m^3).

MIXES	CEMENT	GGBS	UFS	CK	LP	GY	FA	CA	WATER	SP
CONV	575.75	–	–	–	–	–	929.29	721.56	189.99	3.45
HSB0.10	518.17	18.90	37.80	–	–	0.863				3.62
HSB0.20	460.60	37.80	75.61	–	–	1.727				3.45
HSB0.30	403.02	56.71	113.42	–	–	2.59				3.22
HSB0.40	345.45	75.61	151.23	–	–	3.45				2.59
HSB0.50	287.87	94.52	189.04	–	–	4.31				2.01
KLB0.10	518.18	–	–	38	19	0.575				3.63
KLB0.20	460.60	–	–	76	38	1.151				3.22
KLB0.30	403.03	–	–	114	57	1.727				3.02
KLB0.40	345.45	–	–	152	76	2.303				2.59
KLB0.50	287.88	–	–	192	96	2.878				5.75

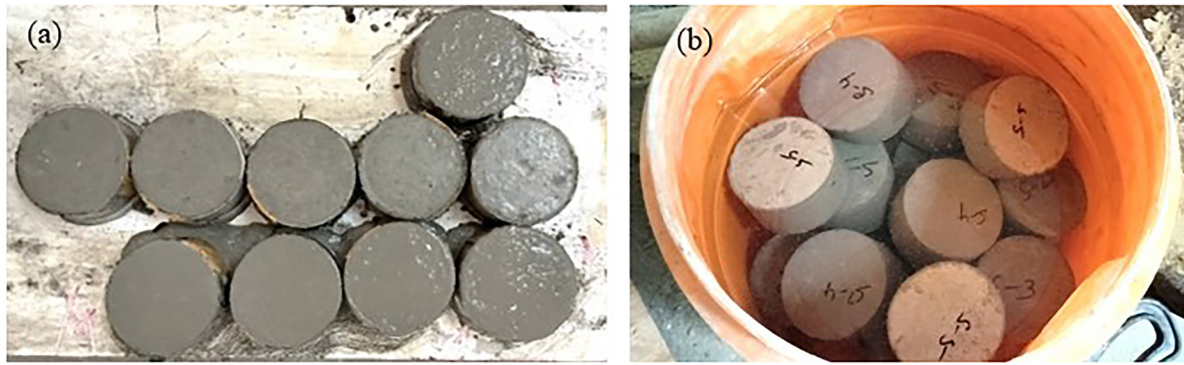


Figure 4: (a) Specimens were cast, (b) Specimens under normal water curing.

Hence, the gypsum content in each blend was carefully optimized to balance setting characteristics and durability in the preparation of the respective tailor-made SCMs. The materials used in this study are shown in Figure 3. Once the fresh properties were satisfied, concrete samples were cast and subjected to standard water curing for 28, 56, and 90 days, respectively, as shown in Figure 4.

3. EXPERIMENTAL INVESTIGATION

To evaluate the durability performance of HS-SCC incorporating tailor-made SCMs, three key tests were conducted that is sorptivity, rapid chloride penetration test, and water absorption test. The cylindrical specimens of 50 mm diameter and 100 mm height were cast and cured under normal water curing for 28, 56, and 90 days. These tests provide a comprehensive understanding of the concrete resistance to moisture ingress and chloride penetration.

3.1. Voids and water absorption characteristics

To investigate the transport properties of high-strength self-compacting concrete, water absorption and porosity were determined as per ASTM C642–13 [27]. These tests provide insights into the pore connectivity and permeability of hardened concrete. Concrete specimens incorporating SCMs were first oven-dried at 100 ± 5 °C until a constant mass was achieved. This oven-dry mass was recorded as (W_d). The specimens were then immersed in water for 48 hours to ensure full saturation, after which the saturated surface-dry mass was recorded as (W_s). Following this, the specimens were boiled in water for 5 hours to simulate accelerated saturation conditions, and the mass after boiling was noted as (W_b). Finally, the specimens were weighed while suspended in water to determine their apparent mass in the submerged state, denoted as (W_{sb}), as illustrated in Figure 5. The water absorption (W_A) was computed as the percentage increase from the oven-dry to saturated surface-dry condition using Equation 1. The water absorption after boiling (W_{BO}) was determined based on the percentage increase from the oven-dry to boiled saturated condition using Equation 2. The volume of permeable voids (V) representing the accessible pore space was calculated using Equation 3.

$$W_A = (W_s - W_d) / W_d * 100 \quad (1)$$

$$W_{BO} = (W_b - W_d) / W_d * 100 \quad (2)$$

$$V = (W_b - W_d) / (W_b - W_{sb}) * 100 \quad (3)$$

3.2. Water sorption characteristics

The sorptivity test evaluates the rate of water ingress into concrete due to capillary suction under unsaturated conditions, which directly reflects the pore structure and connectivity of the matrix [28]. It is a key indicator of the transport properties and potential durability of concrete. The test was performed in accordance with ASTM C1585-20 [29], which prescribes the measurement of cumulative water absorption at multiple time intervals: 5, 10, 20, 30, 60, 120, 180, 240, 300, 360, 1440, 2880, 4320, 7200, 8640, and 10080 minutes. Water absorption due to capillary action was calculated using Equation 4. Where I , Δm , a , represents the absorption (mm), the change in mass (g), the exposed area of the specimen (mm^2), and the density of water (g/mm^3).

$$I = \Delta m / (a * \rho) \quad (4)$$

Table 4: Chloride ion penetrability classification based on charge passed (ASTM C1202-12).

CHARGE PASSED (COULOMBS)	CHLORIDE ION PENETRABILITY
>4,000	High
2,000–4,000	Moderate
1,000–2,000	Low
100–1,000	Very Low
<100	Negligible

The sorptivity coefficient was then determined by plotting the absorbed water per unit area against the square root of time, and calculating the slope of the linear portion of the curve.

3.3. Resistance to chloride permeability

The chloride ion penetration resistance of concrete was assessed using the Rapid Chloride Penetration Test (RCPT), as per ASTM C1202–12 [30]. This test quantifies the concrete's ability to resist chloride ion ingress, a key durability concern for structures exposed to marine environments. The electrical resistivity measured during the test is indicative of the concrete's pore structure and overall permeability. Cylindrical specimens measuring 100 mm in diameter and 50 mm in thickness were cast and water-cured for 28, 56, and 90 days. Before testing, all specimens were placed in a vacuum desiccator. During the test, a constant DC voltage of 60V was applied across the specimen for 6 hours. One face of the specimen was exposed to a 3% NaCl solution, while the opposite face was exposed to a 0.3 N NaOH solution. The total charge passed through the specimen, measured in coulombs, was recorded. The measured charge was then used to classify the chloride ion penetrability of the concrete as listed in Table 4, as defined by ASTM standards.

**Figure 5:** Experimental setup (a) sorptivity, (b) RCPT, (c) submerged specimens, (d) overdried specimens, (e) boiling specimens.

3.4. Microstructural characteristics

The microstructural behavior of concrete incorporating HSB and KLB binder systems was evaluated using Scanning Electron Microscopy (SEM), X-ray Diffraction (XRD), and Fourier Transform Infrared Spectroscopy

(FTIR). SEM was employed to examine the morphology and microcrack patterns of fractured surfaces from hardened core specimens. Samples were crushed below 12 mm, gold-coated, and imaged to observe the distribution of hydration products and matrix densification. XRD analysis was conducted on powdered samples to identify crystalline phases and quantify hydration progression. These phases were tracked through peak intensities in the 2θ range, providing insight into the pozzolanic activity and phase transformations. FTIR spectroscopy was used to examine the chemical bonds and functional groups associated with hydration products. Combined, these techniques provided a comprehensive understanding of hydration mechanisms and durability implications in both HSB and KLB systems.

4. RESULTS AND DISCUSSION

4.1. Voids and water absorption characteristics

The transport characteristics of SCC were evaluated using water absorption (W_A), water absorption after boiling (W_{BO}), and volume of permeable voids (VPV) following ASTM C642. These tests provide critical insights into the water resistance and long-term durability of concrete [31]. The mix designs for all SCC blends were finalized only after satisfying essential fresh property criteria such as flowability, filling ability, and passing ability. This ensures proper compaction and homogeneity, which are closely linked to lower porosity and enhanced resistance to fluid ingress because good fresh properties enhance packing density, which in turn reduces interconnected voids and capillary suction, thereby improving durability [32]. The HSB-modified SCC exhibited a significant reduction in W_A , W_{BO} , and VPV values up to 30% replacement, indicating improved pore refinement and reduced permeability. The lowest W_A of 0.96% and W_{BO} of 0.526% were recorded for HSB0.30 at 90 days, highlighting the synergistic effect of UFS and GGBS in densifying the microstructure and reducing water accessible pores. Beyond 30% replacement, a slight increase in W_A and VPV was observed as listed in Table 5, which correlates with SEM images showing more pore formation and microstructural discontinuities at higher HSB levels as shown in Figure 6(a). This trend aligns with findings by SAGAR and SIVAKUMAR [33] observed that Af addition up to 10% reduced porosity and water absorption due to a denser hardened matrix, while exceeding 12% to 14% led to increased porosity likely due to unreacted lime and micro-crack formation.

Despite the slight rise, HSB0.50 still performed better than the CONV, affirming its superior performance even at higher replacement levels. In contrast, the KLB-based SCC mixes showed a steady reduction in W_A , W_{BO} , and VPV across all replacement levels up to 50%, as shown in Figure 7. The KLB0.50 mix achieved the lowest WA of 1.1069% and W_{BO} 0.2898% at 90 days, confirming superior microstructural densification and minimal void connectivity as shown in Figure 6(c). This improvement is attributed to the pozzolanic activity of CK and the filler and nucleation effects of LP. Together, these materials enhance hydration, promote additional CSH formation, and fill capillary pores, resulting in a dense, refined pore network [34–35]. CHEN *et al.*, [36] observed that limestone additions up to 8% reduced water permeability due to its filler effect. Similarly, 10% limestone addition was optimal for reducing W_A , primarily because of its nucleation, dilution, and filler effects [37]. PRITHIVIRAJ *et al.* [38] observed that increasing Af from 10% to 60% reduced W_A from 0.242% to 0.170% and VPV from 0.674% to 0.546%, due to ultrafine particles filling micro voids and enhancing matrix density. The role of hydration and mineral additives in influencing transport properties is critical. Hydration products and pozzolanic reactions block interconnected pores, narrow capillary channels, and complicate the movement of water, thereby reducing permeability [39].

Table 5: Water absorption.

TESTS	AGES	MIXES										
		CONV	HSB0.10	HSB0.20	HSB0.30	HSB0.40	HSB0.50	KLB0.10	KLB0.20	KLB0.30	KLB0.40	KLB0.50
W_A	28	1.929	1.375	1.315	1.289	1.306	1.388	1.746	1.629	1.561	1.409	1.382
	56	1.750	1.297	1.182	1.055	1.145	1.250	1.529	1.478	1.385	1.273	1.247
	90	1.625	1.206	1.101	0.957	1.117	1.216	1.462	1.368	1.286	1.146	1.106
W_{BO}	28	1.287	1.244	0.889	0.654	0.737	1.110	1.114	0.921	0.912	0.734	0.578
	56	0.956	0.842	0.771	0.576	0.612	0.755	0.923	0.831	0.727	0.623	0.437
	90	0.833	0.735	0.684	0.526	0.624	0.695	0.798	0.625	0.563	0.489	0.289

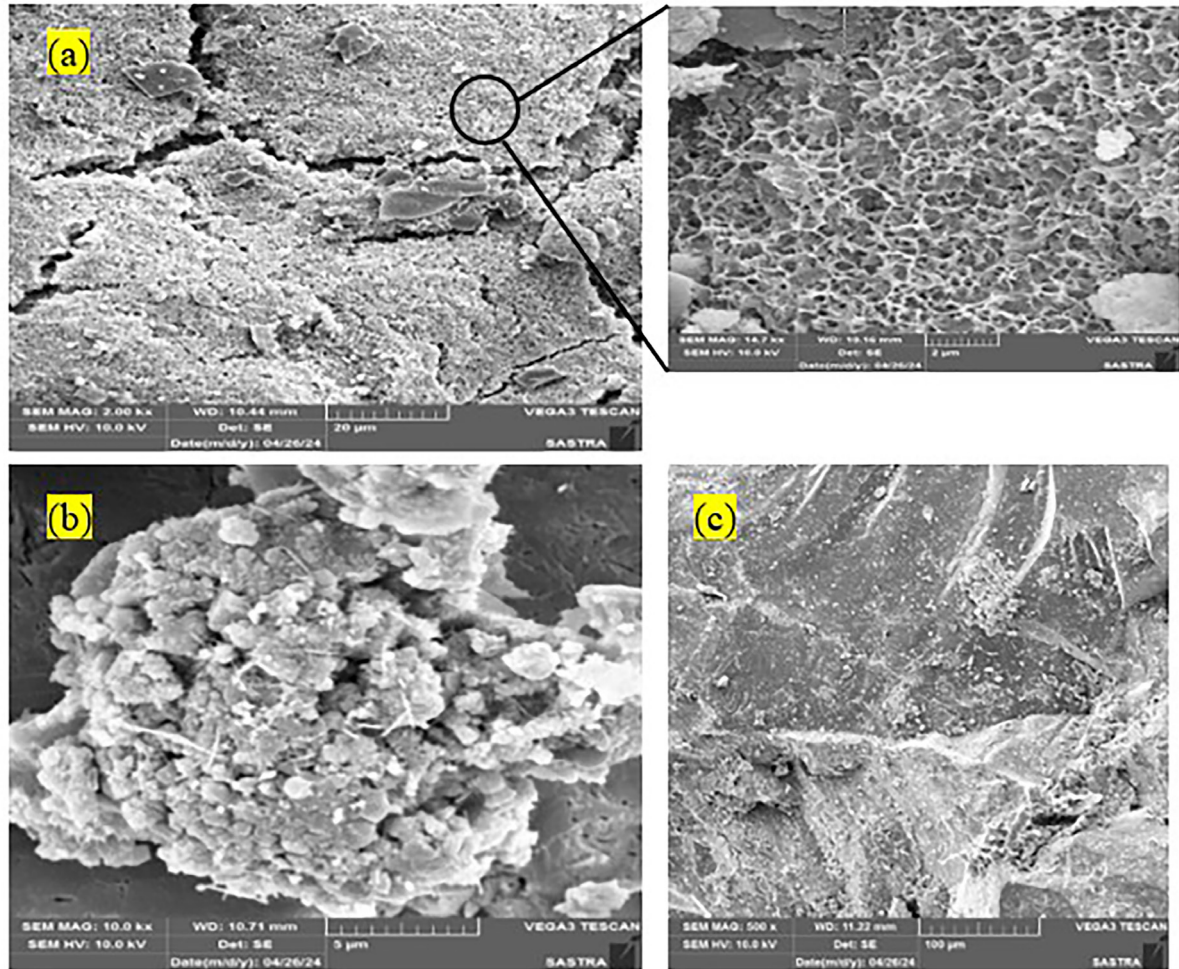


Figure 6: Scanning electron microscopy images.

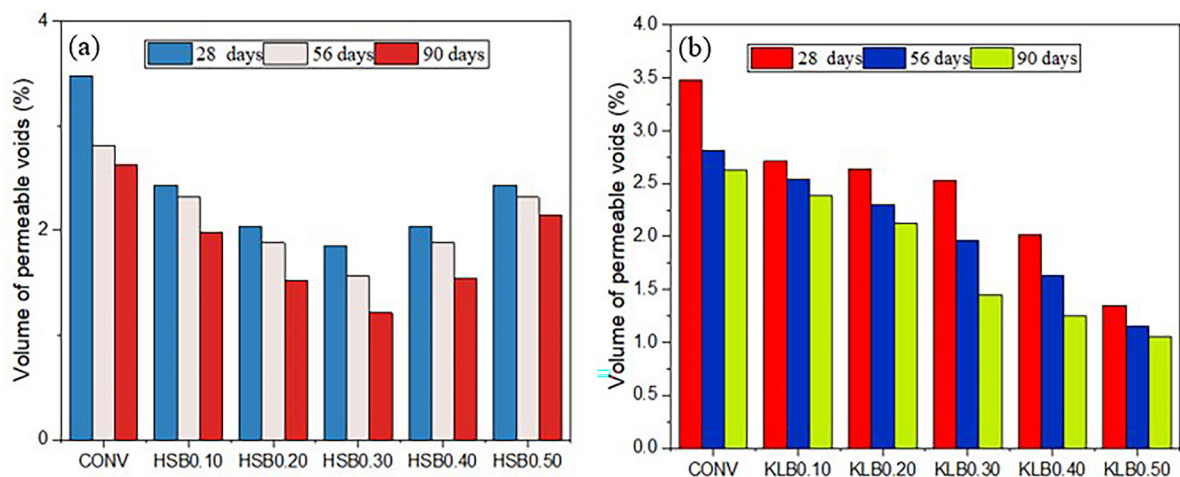


Figure 7: Volume of permeable voids (a) HSB mixes, (b) KLB mixes.

4.2. Water sorption characteristics

Sorptivity, which quantifies the rate of capillary suction in unsaturated concrete, is a key indicator of pore connectivity [40–41]. Higher values indicate a more porous microstructure and reduced resistance to fluid ingress. In this study, sorptivity results mirrored the trends observed in water absorption and permeable voids. From Figure 8, both HSB and KLB-based SCC mixes exhibited a consistent reduction in sorptivity with increasing curing age, reflecting the progressive refinement of pore structure over time. For HSB-SCC, the sorptivity index

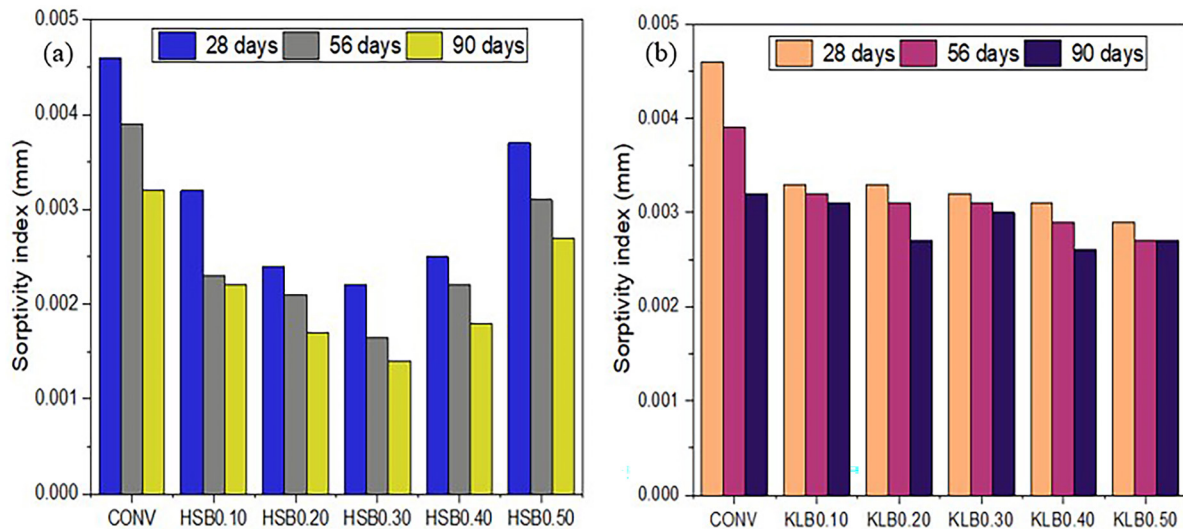


Figure 8: Sorptivity index (a) HSB mixes (b) KLB mixes.

declined as replacement increased up to 30%, beyond which a slight increase was observed. The lowest values were recorded for HSB0.30, with 0.002 mm, 0.0016 mm, and 0.0014 mm at 28, 56, and 90 days, respectively. This reduction is attributed to the enhanced gel formation due to the synergistic effect between Af and GGBS, which densified the matrix and limited capillary continuity. However, at 50% replacement (HSB0.50), sorptivity increased slightly to 0.0037 mm (28 days), 0.0031 mm (56 days), and 0.0027 mm (90 days), which is still lower than the control mix.

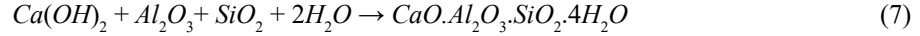
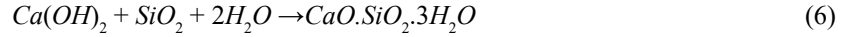
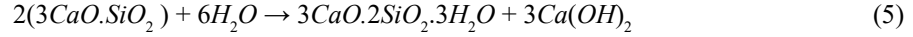
CHEN *et al.* [42] reported that SF exhibited greater reduction in capillary suction and improved durability compared to GGBS when used individually and in combination with SF. The marginal rise is likely due to the dilution effect at higher replacement levels (30%), where excess Af acts primarily as a filler with limited contribution to further hydration, reducing the extent of pore blocking by its physical packing rather than chemical densification [43]. In contrast, KLB-SCC showed a steady and consistent decline in sorptivity with increasing replacement up to 50%. The KLB0.50 mix exhibited values of 0.0029 mm, 0.0027 mm, and 0.0027 mm at 28, 56, and 90 days, respectively. This continuous improvement is attributed to the combined effect of calcined kaolin's pozzolanic reactivity and limestone powder's filler and nucleation roles, which enhanced the formation of secondary C-S-H and refined the pore network as shown in Figure 6(b). KARATAS *et al.* [44] reported that while kaolin addition from 5% to 20% reduced sorptivity compared to the control mix but the use of calcined kaolin showed a slightly higher sorptivity coefficient. However, in the present study, the combination of CK and LP significantly improved resistance to fluid transport, indicating good compatibility and effective pore structure refinement. Comparatively, HSB0.30 achieved the lowest sorptivity overall, while KLB0.50 demonstrated more consistent long-term performance at higher replacement levels.

4.3. Resistance to chloride penetration

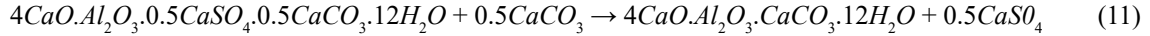
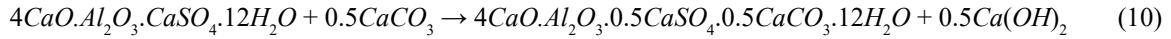
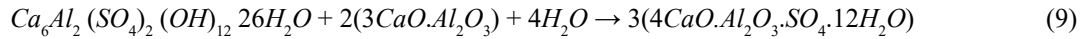
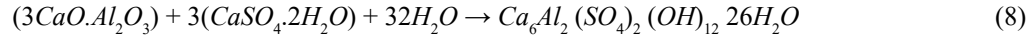
Chloride ingress, a major cause of steel corrosion in concrete, occurs via permeation, diffusion, and capillary absorption, exploiting the pore network or cracks [45], [46]. Even inland structures are vulnerable due to airborne chloride deposition. In SCC, the addition of SCMs significantly alters chloride permeability compared to conventional concrete [47]. In this study, both HSB-SCC and KLB-SCC exhibited very low to negligible chloride permeability across all curing ages, confirming their enhanced durability. This improvement is primarily due to microstructural densification and chloride-binding through Friedel's salt formation, enabled by gypsum reacting with aluminates to form calcium chloroaluminate hydrates [48]. Ghrici, *et al.* [49] limestone powder (LP) can reduce chloride binding at high levels due to the formation of stable carbonates over Friedel's salt. As Gibbs free energy for Friedel's salt is higher than carbonates formed in concrete, therefore, more stable components like carbonates formed by the addition of LP instead of Friedel salt, thereby reducing the extent of chloride binding with the aluminum phases [50].

The presence of calcined kaolin in KLB offsets this by contributing reactive alumina for CASH formation, enhancing ionic resistance. In HSB mixes, GGBS and UFS react with $\text{Ca}(\text{OH})_2$ (portlandite) to form additional CSH and CASH gels, improving pore blocking as per equations 5, 6, and 7. The alumina-rich environment leads to higher chloride binding capacity due to the layered structure of CASH [51]. In HSB-SCC, the charge passed

decreased from 268 to 197 coulombs at 28 days, 248 to 105 coulombs at 56 days, and 204 to 79 coulombs at 90 days from CONV to HSB0.30. HSB0.50 showed slightly higher values than HSB0.30 but remained better than CONV. In KLB-SCC, a consistent reduction was observed at 28 days from 162.4 to 98.62 coulombs, at 56 days from 142.32 to 96.56 coulombs, and 90 days from 121.25 to 92.88 coulombs, with KLB0.50 achieving negligible permeability as shown in Figure 9.



Early-age gypsum addition delayed flash setting by ettringite formation as explained in Equation 8. At higher HSB levels, gypsum depletion and excess alumina promoted porous sulfate phase formation, slightly compromising long-term durability [52] as per Equation 9. But KLB mixes converted the sulphate phase to stable carboaluminates by the LP interaction, as denoted by Equations 10 and 11, enhancing durability [53]. Thus, both blends improved chloride resistance, with HSB effective up to 30% and KLB sustaining performance up to 50%, validating their suitability for durable SCC applications.



4.4. X-ray diffraction

The X-ray diffraction (XRD) analysis provides crucial insight into the mineralogical transformations and hydration behavior induced by varying levels of cement replacement. In CONV and at HSB0.10, the diffraction peaks for portlandite were observed at $2\theta = 18.12^\circ$ and 34.15° , indicating unconsumed calcium hydroxide from the hydration of alite and belite. As the replacement level increased beyond 20%, Portlandite peaks reduced and became undetectable in HSB0.40 and HSB0.50, as shown in Figure 10. This disappearance confirms the effective pozzolanic activity of Af and GGBS, whose high reactivity with Portlandite led to the formation of additional

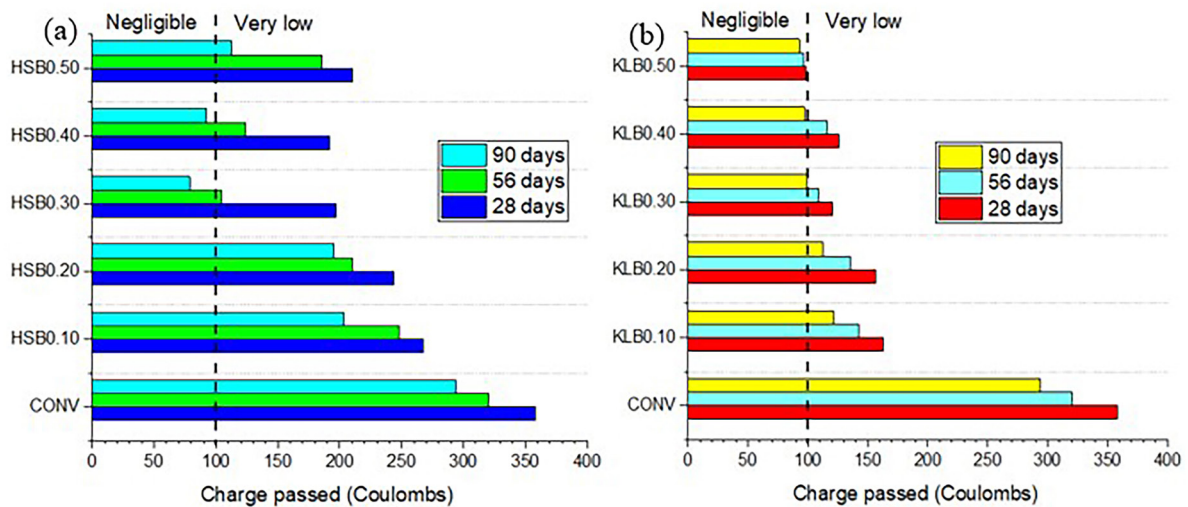


Figure 9: Rapid chloride penetration test (a) HSB mixes, (b) KLB mixes.

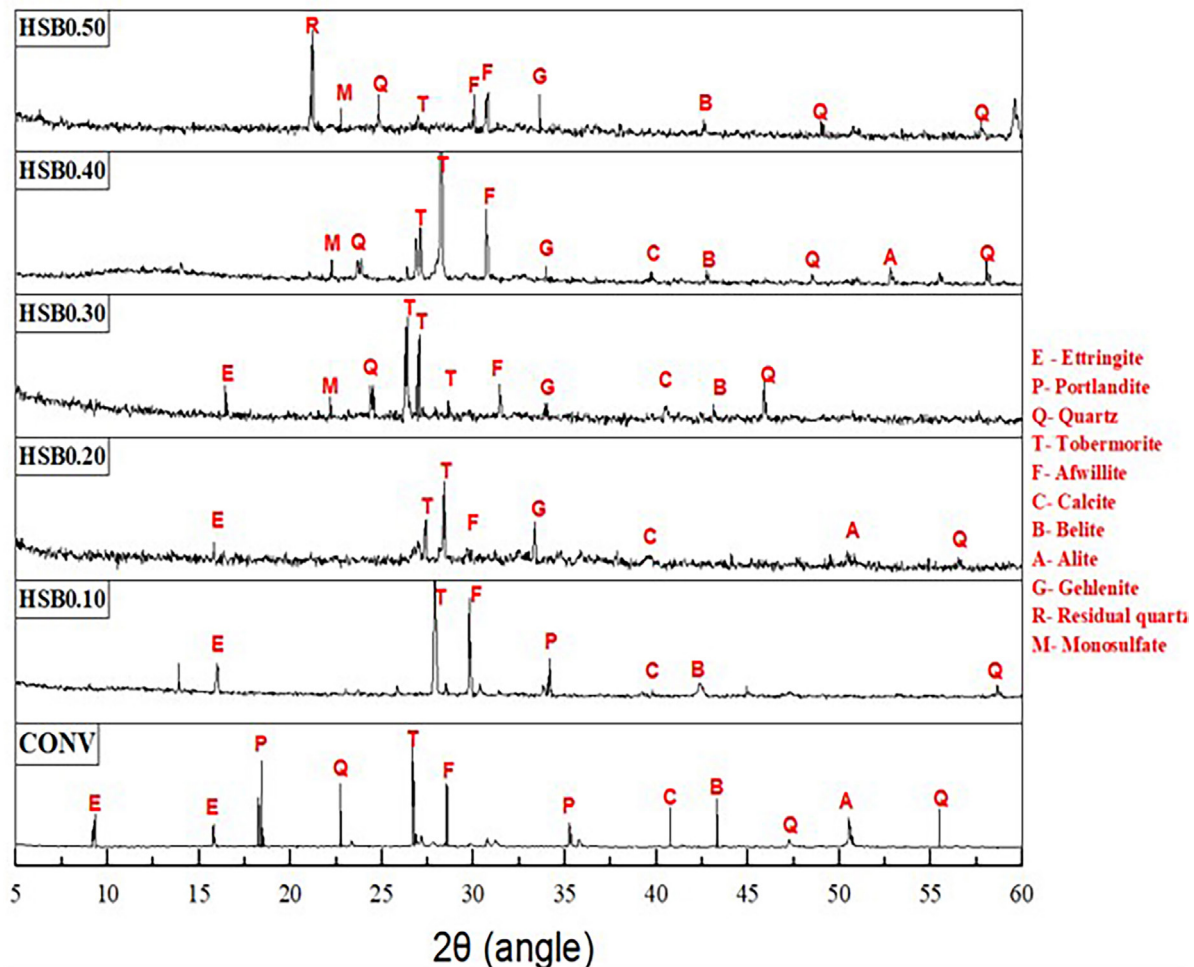


Figure 10: XRD for HSB mixes.

CSH and CASH phases, enhancing matrix densification. The reduction in available portlandite also limits the carbonation process that typically leads to calcite formation, which explains the observed decline in calcite peak intensity with increasing HSB content. The intensity of crystalline CSH phases, especially tobermorite and afwillite, identified between $2\theta = 29^\circ$ and 31° [54], showed increasing intensity with replacement up to HSB0.40, indicating optimal gel development and improved microstructural integrity. However, at HSB0.50, the decline in peak intensity reflects limited C-S-H formation due to insufficient calcium content, thereby explaining the drop in mechanical performance. Prominent gehlenite peaks at $2\theta = 33^\circ$ – 34° in HSB0.20 and HSB0.50 indicate unhydrated slag due to incomplete reaction at higher replacements [55]. The absence of strätlingite in HSB0.50 suggests limited interaction between calcium and aluminum, which may affect the formation of certain stable hydration phases. However, the development of other phases appears to refine the pore structure, contributing to the observed improvement in chloride resistance [56]. Residual quartz peaks at 21.2° confirm the inert nature of part of the blend. Additionally, intensified monosulfate peaks at 22° in HSB0.50 indicate the formation of porous, unstable phases, which contribute to reduced durability at higher substitution levels.

In KLB mixes, a distinct peak at $2\theta = 21.5^\circ$ indicates stratlingite formation, which is a stable hydration product rich in alumina because of the active participation of CK contributed significantly to the pozzolanic reactions in the blend [57]. As the KLB replacement level increased, a noticeable decline in Portlandite peaks ranging from 34.21° to 46.52° was observed, confirming the effective development of secondary hydration products as shown in Figure 11. The formation of ettringite, characterized by peaks between 9° and 10° , became more prominent at higher replacement levels, particularly due to the presence of gypsum [58]. SEM observations supported this, showing dense needle-like ettringite structures in KLB0.50, which may pose durability concerns over time due to their expansive nature, as shown in Figure 6(b). However, this was counterbalanced by the presence of carboaluminate phases at higher replacements. These phases, stabilized by the limestone powder, signify the conversion of less stable ettringite into more durable forms. Furthermore, the disappearance of alite

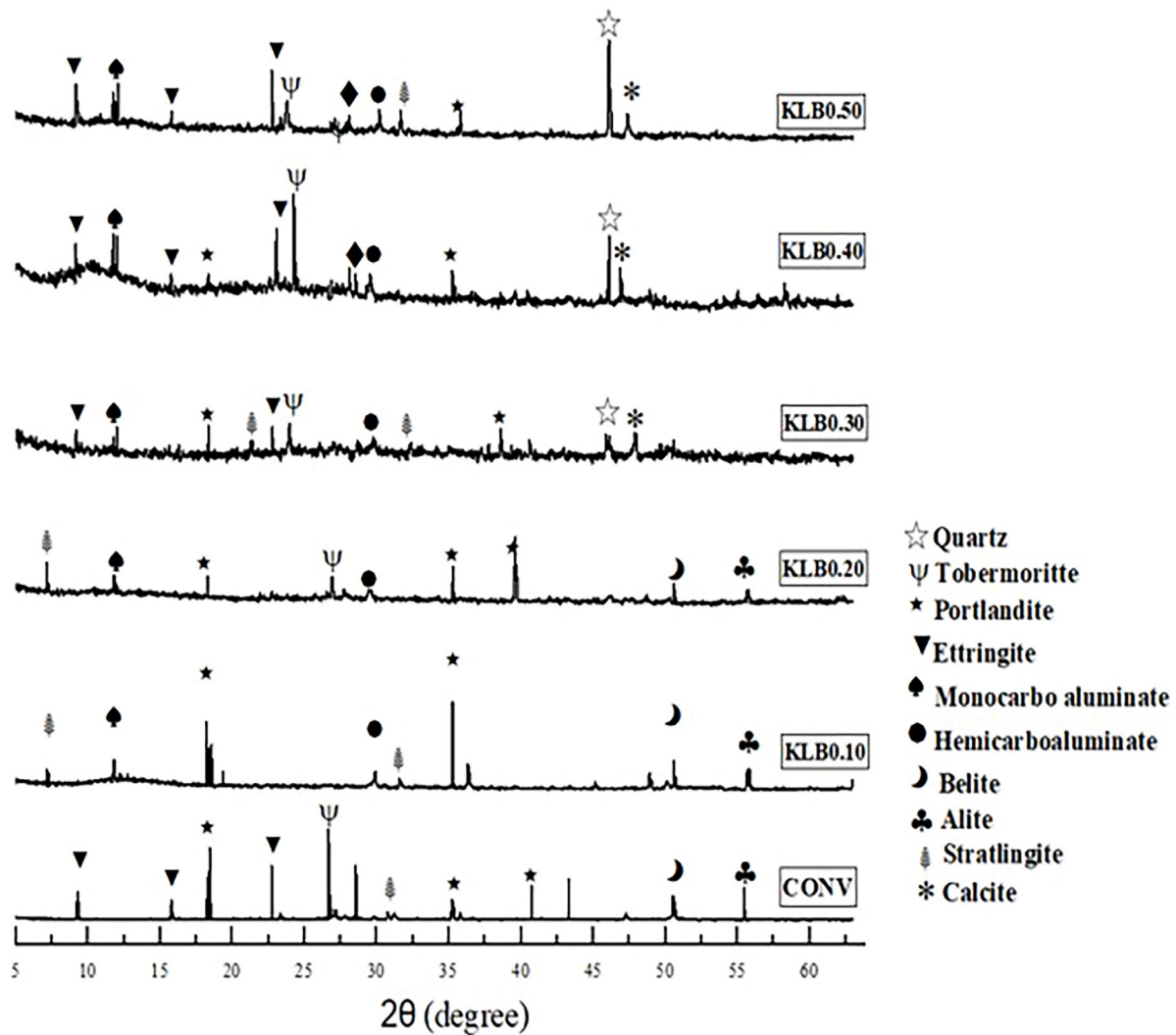


Figure 11: XRD for KLB mixes.

and belite peaks between 51.7° and 55.23° at higher KLB levels indicates a substantial reduction in clinker content, aligned sustainable goal of the blend. Importantly, the peak for mono-carboaluminate at 2θ around 11.9° became more defined in KLB0.40 and KLB0.50, while the hemicarboaluminate peak at 28.95° diminished [59]. This shift suggests a transition toward more stable sulfate-bearing phases, enhancing the sulfate resistance and durability of the system even at higher replacement levels.

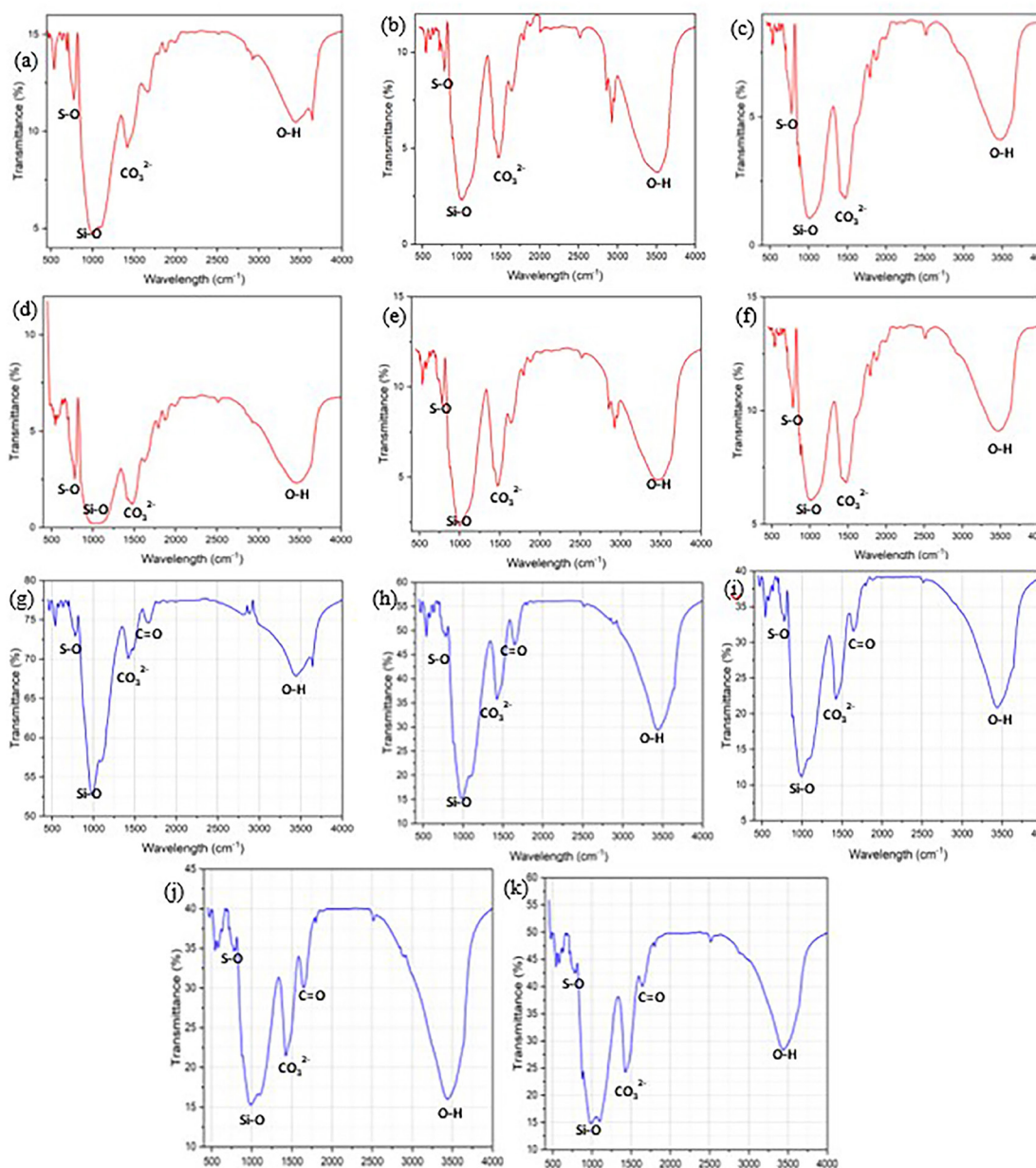
4.5. Fourier transform infrared spectroscopy

The FTIR spectra of the HSB and KLB mixes, as shown in Figure 12, provide insights into the chemical composition and hydration mechanisms of the blends. The specific absorption bands and their corresponding functional groups are detailed in Table 6.

A broad absorption band between $3650\text{--}3400\text{ cm}^{-1}$ was observed in all samples, corresponding to the O–H stretching vibrations of structural hydroxyl groups and adsorbed water molecules, including those in ettringite. In the CONV, a sharp peak around 3640 cm^{-1} indicates strong O–H stretching, signifying the presence of portlandite and bound water during early hydration [61]. In the region between $1300\text{--}1500\text{ cm}^{-1}$, C–O stretching vibrations of carbonate ions (CO_3^{2-}) were evident, indicating the presence of carbonate-related phases [62]. In HSB mixes, the transmittance of this band increased slightly with higher replacement levels, suggesting a reduction in carbonate bond intensity and hence lower formation of carboaluminate phases. In contrast, the KLB mixes showed a decrease in transmittance in this range with increasing replacement, signifying stronger carbonate bonding and the formation of stable carboaluminate phases, a beneficial factor for long-term durability [63].

Table 6: Analysis of functional group absorption characteristics in the FTIR spectra [60].

ABSORPTION BAND (cm^{-1})	VIBRATIONAL MODE	INTERPRETATION
3642–3637	vs (OH)Al	$[\text{Al}(\text{OH})_6]^{3-}$
3432–3428	vas (OH)w	H_2O
1676–1621	δ (H–O–H)	H_2O
1496–1363	ν C–O	CO_3^{2-}
1169	vas S–O	SO_4^{2-} (monosulfate)
1115, 1113, 1108	vas S–O	SO_4^{2-} (ettringite)
989, 988, 983	vs S–O	SO_4^{2-}
860–616	δ Al–O–H	$[\text{Al}(\text{OH})_6]^{3-}$
594	Octahedral Al	$[\text{AlO}_6]$ in AFm
540–534	ν S–O	SO_4^{2-} (ettringite)
421–420	δ Al–O–H, δ O–Al–O	$[\text{Al}(\text{OH})_6]^{3-}$

**Figure 12:** FTIR for HSB and KLB mixes.

The Si–O asymmetric stretching vibrations observed between 1000–1250 cm⁻¹ showed marked differences between the mixes. In HSB blends, narrowing and reduced intensity of this peak at higher replacement levels indicated reduced reactivity of the slag components and limited gel formation. Conversely, in the KLB series, a noticeable shift and sharpening of the Si–O band with increasing KLB content suggested higher pozzolanic reactivity, resulting in a denser microstructure and enhanced durability [64]. At lower wave numbers, bands at 618 cm⁻¹ and 540 cm⁻¹ were associated with the stretching vibrations of S–O bonds, characteristic of ettringite. These peaks were more intense in lower KLB replacements but diminished significantly at higher levels, indicating a decline in sulfate phases and the stabilization of carboaluminates through the action of limestone powder [65]. This transition supports the interpretation that the combination of CK and LP encourages the formation of durable hydration products while mitigating the risk of sulfate-induced expansion.

Overall, the FTIR results confirm that KLB mixes, particularly at higher replacement levels, promote the formation of stable carboaluminate phases and reduce sulfate phases, contributing to a more durable microstructure. In contrast, higher replacement levels in HSB mixes resulted in reduced silicate reactivity and lower formation of hydration gels, aligning with the trends observed in durability performance.

5. CONCLUSIONS

In high-strength self-compacting concrete (HS-SCC), replacing cement with hybrid slag blend (HSB) and kaolinite-limestone blend (KLB) as tailored supplementary cementitious materials (SCMs), the following conclusions are drawn concerning durability properties:

- The incorporation of HSB and KLB blends enhanced the durability of SCC by refining the pore network and improving microstructural density. A 30% HSB replacement reduced the volume of permeable voids by 46.84% at 28 days and 53.71% at 90 days compared to the CONV.
- Even at 50% HSB, the voids reduced by 30.09% at 28 days and 18.25% at 90 days compared to CONV, though slightly diminished due to the presence of unhydrated particles and porous monosulfate phases.
- KLB blends demonstrated consistent improvement with increasing replacement. At 50% replacement, void volume dropped by 61.11% and 59.94% at 28 and 90 days, respectively, compared to CONV. This was attributed to the formation of stable carboaluminate phases, replacement of porous sulfates.
- The alumina-rich composition in the KLB formulation enhanced chloride-binding capacity, while XRD results confirmed clinker phase reduction, supporting its effectiveness as a sustainable cement replacement.
- While moderate HSB enhanced particle packing, excessive ultrafine content hindered hydration due to calcium hydroxide deficiency. In contrast, KLB blends sustained reactivity and structural refinement even at higher dosages.
- A tailor-made SCM comprising CK of 32.67%, LP of 16.33%, and gypsum of 1% that conglomerates 50% KLB in SCC as a partial cement replacement is suggested for high-strength & high-performance SCC.

6. ACKNOWLEDGMENTS

The authors gratefully acknowledge the support provided by the management of SASTRA Deemed University.

7. BIBLIOGRAPHY

- [1] RAJAMANICKAM, G., VAIYAPURI, R., “Evaluation of self compacting concrete performance incorporated with presoaked lightweight aggregates”, *Matéria*, v. 30, n. 1, pp. e20240813, Feb. 2025. doi: <http://doi.org/10.1590/1517-7076-rmat-2024-0813>.
- [2] VADAMALAI, P., PARAMASIVAM, S.K., “Performance analysis of bacterial self-compacting concrete – workability, mechanical, durability and micro analysis”, *Matéria*, v. 29, n. 1, pp. e20230238, Jan. 2024. doi: <http://doi.org/10.1590/1517-7076-RMAT-2023-0238>.
- [3] DIAMOND, S., “Mercury porosimetry”, *Cement and Concrete Research*, v. 30, n. 10, pp. 1517–1525, Oct. 2000. doi: [http://doi.org/10.1016/S0008-8846\(00\)00370-7](http://doi.org/10.1016/S0008-8846(00)00370-7).
- [4] YE, G., “Percolation of capillary pores in hardening cement pastes”, *Cement and Concrete Research*, v. 35, n. 1, pp. 167–176, Jan. 2005. doi: <http://doi.org/10.1016/j.cemconres.2004.07.033>.
- [5] ULRIK NILSEN, A., MONTEIRO, P.J.M., “Concrete: a three phase material”, *Cement and Concrete Research*, v. 23, n. 1, pp. 147–151, Jan. 1993. doi: [http://doi.org/10.1016/0008-8846\(93\)90145-Y](http://doi.org/10.1016/0008-8846(93)90145-Y).
- [6] NIKZAD, Y., MAZLOOM, M., PARHIZKARI, M.H., “Effect of sand fineness modulus on SCC and SCLC properties”, *Construction & Building Materials*, v. 421, pp. 135761, Mar. 2024. doi: <http://doi.org/10.1016/j.conbuildmat.2024.135761>.

- [7] MOHAN, A., MINI, K.M., “Strength and durability studies of SCC incorporating silica fume and ultra fine GGBS”, *Construction & Building Materials*, v. 171, pp. 919–928, 2018. doi: <http://doi.org/10.1016/j.conbuildmat.2018.03.186>.
- [8] UYSAL, M., SUMER, M., “Performance of self-compacting concrete containing different mineral admixtures”, *Construction & Building Materials*, v. 25, n. 11, pp. 4112–4120, Nov. 2011. doi: <http://doi.org/10.1016/j.conbuildmat.2011.04.032>.
- [9] DEVI, S.S., VIVEK, S.S., “Self-compacting concrete using supplementary cementitious materials and fibers.”, *Civil Engineering*, v. 48, n. 6, pp. 3899–3925, 2024. doi: <http://doi.org/10.1007/s40996-024-01414-9>.
- [10] ARUMUGAM, C., THIRUMALA, G.K.G.V., RAJAMANICKAM, G., “Investigations on self-compacting concrete utilizing agricultural waste ashes”, *Matéria*, v. 30, pp. e20240860, 2025. doi: <http://doi.org/10.1590/1517-7076-rmat-2024-0860>.
- [11] JURADIN, S., VLAJIĆ, D., “Influence of Cement Type and Mineral Additions, Silica Fume and Metakaolin, on the Properties of Fresh and Hardened Self-compacting Concrete”, In: Ochsner, A., Altenbach, H. (eds), *Mechanical and Materials Engineering of Modern Structure and Component Design*, Cham, Springer, 2015. doi: http://doi.org/10.1007/978-3-319-19443-1_20.
- [12] CHANDRU, P., KARTHIKEYAN, J., SAHU, *et al.*, “Performance evaluation between ternary blended SCC mixes containing induction furnace slag and crushed stone as coarse aggregate”, *Construction & Building Materials*, v. 267, pp. 120953, Jan. 2021. doi: <http://doi.org/10.1016/j.conbuildmat.2020.120953>.
- [13] CHANDRU, P., KARTHIKEYAN, J., SAHU, *et al.*, “Some durability characteristics of ternary blended SCC containing crushed stone and induction furnace slag as coarse aggregate”, *Construction & Building Materials*, v. 270, pp. 121483, Feb. 2021. doi: <http://doi.org/10.1016/j.conbuildmat.2020.121483>.
- [14] WONGKEO, W., THONGSANITGARN, P., NGAMJARUROJANA, A., *et al.*, “Compressive strength and chloride resistance of self-compacting concrete containing high level fly ash and silica fume”, *Materials & Design*, v. 64, pp. 261–269, Dec. 2014. doi: <http://doi.org/10.1016/j.matdes.2014.07.042>.
- [15] BIRGONDA, S., KARTHIKEYAN, J., “Comparative analysis of quaternary blended self-compacting concrete (QBSCC) mixes incorporating induction furnace slag (IFS) and crushed stone aggregate: a performance study”, *Journal of Building Engineering*, v. 76, pp. 107386, Oct. 2023. doi: <http://doi.org/10.1016/j.jobe.2023.107386>.
- [16] BIRGONDA, S., SENTHILKUMAR, R., RAMESH, S.T., “Induction furnace slag as fine and coarse aggregate in quaternary blended self-compacting concrete: a comprehensive study on durability and performance”, *Materials Today Sustainability*, v. 27, pp. 100873, Sep. 2024. doi: <http://doi.org/10.1016/j.mtsust.2024.100873>.
- [17] BIRGONDA, S., SENTHILKUMAR, R., RAMESH, S.T., “Long-term performance and phase characterization of Quaternary Blended Self-Compacting Concrete incorporating IFSS aggregates: a multidisciplinary investigation.”, *Journal of Building Engineering*, v. 102, pp. 111966, 2025. doi: <http://doi.org/10.1016/j.jobe.2025.111966>.
- [18] JUENGER, M., PROVIS, J.L., ELSEIN, J., *et al.*, “Supplementary cementitious materials for concrete: Characterization needs”, *Materials Research Society*, v. 88, pp. 22, Jan. 2013.
- [19] BUREAU OF INDIAN STANDARDS, *IS 12269, Ordinary Portland Cement, 53 Grade - Specifications (first review)*, New Delhi, Bureau of Indian Standards, 2013.
- [20] BUREAU OF INDIAN STANDARDS, *IS 383, Coarse and Fine Aggregate for Concrete – Specification*, New Delhi, Bureau of Indian Standards, 2016.
- [21] AMERICAN SOCIETY FOR TESTING AND MATERIALS, *ASTM C494 Standard Specification for Chemical Admixtures for Concrete*, West Conshohocken, ASTM, 2017.
- [22] BUREAU OF INDIAN STANDARDS, *IS 10262, Concrete Mix Proportioning-Guidelines*, 2 ed, New Delhi, Bureau of Indian Standards, 2019.
- [23] THE EUROPEAN GUIDELINES FOR SELF-COMPACTING CONCRETE SPECIFICATION, *Production and Use ‘The European Guidelines for Self Compacting Concrete*, Evergem, EFCA, 2005.
- [24] GYABAAH, G., MIYAZAWA, S., NITO, N., “Effects of gypsum and limestone powder on fresh properties and compressive strength of concrete containing ground granulated blast furnace slag under different curing temperatures”, *Construction Materials*, v. 2, n. 2, pp. 114–126, Jun. 2022. doi: <http://doi.org/10.3390/constrmater2020009>.

- [25] SAGAR, B., SIVAKUMAR, M.V.N., “Use of alccofine-1203 in concrete: review on mechanical and durability properties”, *International Journal of Sustainable Engineering*, v. 14, n. 6, pp. 2060–2073, 2021. doi: <http://doi.org/10.1080/19397038.2021.1970275>.
- [26] MOHAMMED, S., SAFIULLAH, O., “Optimization of the SO₃ content of an Algerian Portland cement: study on the effect of various amounts of gypsum on cement properties”, *Construction & Building Materials*, v. 164, pp. 362–370, Mar. 2018. doi: <http://doi.org/10.1016/j.conbuildmat.2017.12.218>.
- [27] AMERICAN SOCIETY FOR TESTING AND MATERIALS, *ASTM C642, Test Method for Density, Absorption, and Voids in Hardened Concrete*, West Conshohocken, ASTM, 2021.
- [28] LEUNG, H.Y., KIM, J., NADEEM, A., *et al.*, “Sorptivity of self-compacting concrete containing fly ash and silica fume”, *Construction & Building Materials*, v. 113, pp. 369–375, Jun. 2016. doi: <http://doi.org/10.1016/j.conbuildmat.2016.03.071>.
- [29] AMERICAN SOCIETY FOR TESTING AND MATERIALS, *ASTM C1585, Test Method for Measurement of Rate of Absorption of Water by Hydraulic-Cement Concretes*, West Conshohocken, ASTM, 2020.
- [30] AMERICAN SOCIETY FOR TESTING AND MATERIALS, *ASTM C1202-12, Test Method for Electrical Indication of Concretes Ability to Resist Chloride Ion Penetration*, West Conshohocken, ASTM, 2012.
- [31] TORRES, M.L., GARCÍA-RUIZ, P.A., “Lightweight pozzolanic materials used in mortars: evaluation of their influence on density, mechanical strength and water absorption”, *Cement and Concrete Composites*, v. 31, n. 2, pp. 114–119, Feb. 2009. doi: <http://doi.org/10.1016/j.cemconcomp.2008.11.003>.
- [32] LUHAR, S., LUHAR, I., “Potential application of E-wastes in construction industry: a review”, *Construction & Building Materials*, v. 203, pp. 222–240, Apr. 2019. doi: <http://doi.org/10.1016/j.conbuildmat.2019.01.080>.
- [33] SAGAR, B., SIVAKUMAR, M.V.N., “An experimental and analytical study on alccofine based high strength concrete”, *International Journal of Engineering*, v. 33, n. 4, pp. 530–538, Apr. 2020.
- [34] WANG, W., LIU, X., GUO, L., *et al.*, “Evaluation of properties and microstructure of cement paste blended with metakaolin subjected to high temperatures”, *Materials*, v. 12, n. 6, pp. 941, Mar. 2019. doi: <http://doi.org/10.3390/ma12060941>. PubMed PMID: 30901857.
- [35] MUDULI, R., MUKHARJEE, B.B., “Effect of incorporation of metakaolin and recycled coarse aggregate on properties of concrete”, *Journal of Cleaner Production*, v. 209, pp. 398–414, Feb. 2019. doi: <http://doi.org/10.1016/j.jclepro.2018.10.221>.
- [36] CHEN, J.J., KWAN, A.K.H., JIANG, Y., “Adding limestone fines as cement paste replacement to reduce water permeability and sorptivity of concrete”, *Construction & Building Materials*, v. 56, pp. 87–93, Apr. 2014. doi: <http://doi.org/10.1016/j.conbuildmat.2014.01.066>.
- [37] RAMEZANIANPOUR, A.A., GHIASVAND, E., NICKSERESHT, I., *et al.*, “Influence of various amounts of limestone powder on performance of Portland limestone cement concretes”, *Cement and Concrete Composites*, v. 31, n. 10, pp. 715–720, Nov. 2009. doi: <http://doi.org/10.1016/j.cemconcomp.2009.08.003>.
- [38] PRITHIVIRAJ, C., SARAVANAN, J., RAMESH KUMAR, D., *et al.*, “Assessment of strength and durability properties of self-compacting concrete comprising alccofine”, *Sustainability*, v. 14, n. 10, pp. 5895, 2022. doi: <http://doi.org/10.3390/su14105895>.
- [39] WENZHONG, Z. “Permeation properties of self-compaction concrete”, In: Siddique, R. (ed), *Self-Compacting Concrete: Materials, Properties and Applications*, Sawston, Woodhead Publishing, Elsevier, pp. 117–130, 2020.
- [40] ARUNCHAITANYA, S., DEY, S., “Sorptivity and rapid chloride ion penetration of self-compacting concrete using fly ash and copper slag”, *AI in Civil Engineering*, v. 2, n. 1, pp. 4, Jun. 2023. doi: <http://doi.org/10.1007/s43503-023-00013-3>.
- [41] DIAS, W.P.S., “Reduction of concrete sorptivity with age through carbonation”, *Cement and Concrete Research*, v. 30, n. 8, pp. 1255–1261, Aug. 2000. doi: [http://doi.org/10.1016/S0008-8846\(00\)00311-2](http://doi.org/10.1016/S0008-8846(00)00311-2).
- [42] CHEN, W., WU, M., LIANG, Y., “Effect of SF and GGBS on pore structure and transport properties of concrete”, *Materials*, v. 17, n. 6, pp. 1365, Mar. 2024. doi: <http://doi.org/10.3390/ma17061365>. PubMed PMID: 38541519.
- [43] SRINATH, B. S., PATNAIKUNI, C. K., SANTHOSH, K. B., *et al.*, “Strength effect of alccofine on ordinary and standard grade concrete mixes”, *International Journal of Advanced Technology and Engineering Exploration*, v. 9, n. 86, pp. 47, 2022.

- [44] KARATAS, M., BENLI, A., ARSLAN, F., “The effects of kaolin and calcined kaolin on the durability and mechanical properties of self-compacting mortars subjected to high temperatures”, *Construction & Building Materials*, v. 265, pp. 120300, Dec. 2020. doi: <http://doi.org/10.1016/j.conbuildmat.2020.120300>.
- [45] MCPOLIN, D., BASHEER, P.A.M., LONG, A.E., *et al.*, “Obtaining progressive chloride profiles in cementitious materials”, *Construction & Building Materials*, v. 19, n. 9, pp. 666–673, Nov. 2005. doi: <http://doi.org/10.1016/j.conbuildmat.2005.02.015>.
- [46] ANDRADE, C., WHITING, D., “A comparison of chloride ion diffusion coefficients derived from concentration gradients and non-steady state accelerated ionic migration”, *Materials and Structures*, v. 29, n. 8, pp. 476–484, Oct. 1996. doi: <http://doi.org/10.1007/BF02486282>.
- [47] VEJMELOVÁ, E., KEPPERT, M., GRZESZCZYK, S., *et al.*, “Properties of self-compacting concrete mixtures containing metakaolin and blast furnace slag”, *Construction & Building Materials*, v. 25, n. 3, pp. 1325–1331, Mar. 2011. doi: <http://doi.org/10.1016/j.conbuildmat.2010.09.012>.
- [48] YANG, T., FAN, X., GAO, X., *et al.*, “Modification on the chloride binding capacity of alkali activated slag by applying calcium and aluminium containing phases”, *Construction & Building Materials*, v. 358, pp. 129427, Dec. 2022. doi: <http://doi.org/10.1016/j.conbuildmat.2022.129427>.
- [49] GHRICI, M., KENAI, S., MANSOUR, M.S., “Mechanical properties and durability of mortar and concrete containing natural pozzolana and limestone blended cements”, *Cement and Concrete Composites*, v. 29, n. 7, pp. 542–549, Aug. 2007. doi: <http://doi.org/10.1016/j.cemconcomp.2007.04.009>.
- [50] BAQUERIZO, L.G., MATSCHEI, T., SCRIVENER, K.L., *et al.*, “Hydration states of AFm cement phases”, *Cement and Concrete Research*, v. 73, pp. 143–157, Jul. 2015. doi: <http://doi.org/10.1016/j.cemconres.2015.02.011>.
- [51] AHMAD, J., KONTOLEON, K.J., MAJDI, A., *et al.*, “A comprehensive review on the Ground Granulated Blast Furnace Slag (GGBS) in concrete production”, *Sustainability*, v. 14, n. 14, pp. 8783, Jul. 2022. doi: <http://doi.org/10.3390/su14148783>.
- [52] ELAKNESWARAN, Y., LI, C., KAJIO, T., *et al.*, “Durability of slag-blended cement due to U-phase instability in sulphate environment”, *Materials and Structures*, v. 53, n. 6, pp. 146, Dec. 2020. doi: <http://doi.org/10.1617/s11527-020-01584-8>.
- [53] ZAJAC, M., ROSSBERG, A., SAOUT, G.L., *et al.*, “Influence of limestone and anhydrite on the hydration of Portland cements”, *Cement and Concrete Composites*, v. 46, pp. 99–108, Feb. 2014. doi: <http://doi.org/10.1016/j.cemconcomp.2013.11.007>.
- [54] SHAW, S., CLARK, S.M., HENDERSON, C.M.B., “Hydrothermal formation of the calcium silicate hydrates, tobermorite ($\text{Ca}_5\text{Si}_6\text{O}_{16}(\text{OH})_2 \cdot 4\text{H}_2\text{O}$) and xonotlite ($\text{Ca}_6\text{Si}_6\text{O}_{17}(\text{OH})_2$): an in situ synchrotron study”, *Chemical Geology*, v. 167, n. 1–2, pp. 129–140, Jun. 2000. doi: [http://doi.org/10.1016/S0009-2541\(99\)00205-3](http://doi.org/10.1016/S0009-2541(99)00205-3).
- [55] ZANNI, H., CHEYREZY, M., MARET, V., *et al.*, “Investigation of hydration and pozzolanic reaction in Reactive Powder Concrete (RPC) using ^{29}Si NMR”, *Cement and Concrete Research*, v. 26, n. 1, pp. 93–100, Jan. 1996. doi: [http://doi.org/10.1016/0008-8846\(95\)00197-2](http://doi.org/10.1016/0008-8846(95)00197-2).
- [56] MARPLE, M.A.T., KOROGLU, B., MORRISON, K., *et al.*, “Structural mechanism of carbon mineralization in mechano-chemically alkali activated cementitious materials from granulated slag Cement and Concrete Research”, *Cement and Concrete Research*, Jun. 2020.
- [57] SAGAR, B., SIVAKUMAR, M.V.N., “Mechanical and microstructure characterization of alccofine based high strength concrete”, *Silicon*, v. 14, n. 3, pp. 795–813, Feb. 2022. doi: <http://doi.org/10.1007/s12633-020-00863-x>.
- [58] ZUNINO, F., SCRIVENER, K., “The reaction between metakaolin and limestone and its effect in porosity refinement and mechanical properties”, *Cement and Concrete Research*, v. 140, pp. 106307, Feb. 2021. doi: <http://doi.org/10.1016/j.cemconres.2020.106307>.
- [59] AVET, F., SCRIVENER, K., “Investigation of the calcined kaolin content on the hydration of Limestone Calcined Clay Cement (LC3)”, *Cement and Concrete Research*, v. 107, pp. 124–135, May. 2018. doi: <http://doi.org/10.1016/j.cemconres.2018.02.016>.
- [60] SZUDEK, W., SZYDŁOWSKI, J., BUCHAŁA, I., *et al.*, “Synthesis and characterization of Calcium Sulfoaluminate Hydrates—Ettringite (AFt) and Monosulfate (AFm)”, *Materials*, v. 17, n. 21, pp. 5216, 2024. doi: <http://doi.org/10.3390/ma17215216>. PubMed PMID: 39517493.

- [61] SCHOLTZOVA, E., KUCKOVA, L., KOŽÍŠEK, J., *et al.*, “Structural and spectroscopic characterization of ettringite mineral –combined DFT and experimental study”, *Journal of Molecular Structure*, v. 1100, pp. 215–224, Nov. 2015. doi: <http://doi.org/10.1016/j.molstruc.2015.06.075>.
- [62] KLOPROGGE, J.T., WHARTON, D., HICKEY, L., *et al.*, “Infrared and Raman study of interlayer anions CO 3²⁻, NO 3⁻, SO 4²⁻ and ClO 4⁻ in Mg/Al-hydrotalcite”, *The American Mineralogist*, v. 87, n. 5–6, pp. 623–629, May. 2002. doi: <http://doi.org/10.2138/am-2002-5-604>.
- [63] LOTHENBACH, B., SAOUT, G.L., GALLUCCI, E., *et al.*, “Influence of limestone on the hydration of Portland cements”, *Cement and Concrete Research*, v. 38, n. 6, pp. 848–860, Jun. 2008. doi: <http://doi.org/10.1016/j.cemconres.2008.01.002>.
- [64] ELLERBROCK, R., STEIN, M., SCHALLER, J., “Comparing amorphous silica, short-range-ordered silicates and silicic acid species by FTIR”, *Scientific Reports*, v. 12, n. 1, pp. 11708, Jul. 2022. doi: <http://doi.org/10.1038/s41598-022-15882-4>. PubMed PMID: 35810178.
- [65] TAYLOR, M., BROWN JUNIOR, G.E., “Structure of mineral glasses—I. The feldspar glasses NaAlSi3O8, KAlSi3O8, CaAl2Si2O8”, *Geochimica et Cosmochimica Acta*, v. 43, n. 1, pp. 61–75, Jan. 1979. doi: [http://doi.org/10.1016/0016-7037\(79\)90047-4](http://doi.org/10.1016/0016-7037(79)90047-4).